Supporting Information

Parallelized Ligand Screening Using Dissolution Dynamic Nuclear Polarization

Yaewon Kim, Mengxiao Liu and Christian Hilty*

Department of Chemistry, Texas A&M University, College Station, TX 77843-3255, USA.

*Corresponding author. e-mail: chilty@tamu.edu

Table of Contents

1. Competitive binding of two ligands to a protein

In competitive binding, two ligands bind reversibly to the same position of a protein. When a dissociation constant (K_D) is known for one ligand and it is in fast exchange, it can be used as a reporter ligand to manifest the binding affinity of the other according to the following mechanism.

Competitive Binding Mechanism:

$$CP + R \overset{K_{D,c}}{\rightleftharpoons} R + C + P \overset{K_{D,r}}{\rightleftharpoons} RP + C \tag{S1}$$

R: Reporter ligand
C: Ligand of interest
P: Protein

$K_{D,c}$: Dissociation constant of ligand of interest; $K_{D,c} = \dfrac{[C][P]}{[CP]}$

$K_{D,r}$: Dissociation constant of reporter ligand; $K_{D,r} = \dfrac{[R][P]}{[RP]}$

In relaxation-based NMR experiments, the observed relaxation rate is affected by the relative populations of free and bound reporter ligands. These populations can be calculated by solving the mathematical equations describing the competitive binding of two ligands to a protein. The solution for the fraction of bound reporter ligand was given by Wang:[1]

$$p_b = \frac{2\sqrt{(a^2 - 3b)}\cos(\theta/3) - a}{3K_{D,r} + 2\sqrt{(a^2 - 3b)}\cos(\theta/3) - a} \tag{S2}$$

where

$$\theta = \arccos\left[\frac{-2a^3 + 9ab - 27c}{2\sqrt{(a^2 - 3b)^3}}\right] \tag{S3}$$

and

$$a = K_{D,r} + K_{D,c} + [R]_{tot} + [C]_{tot} - [P]_{tot} \tag{S4}$$

$$b = K_{D,c}([R]_{tot} - [P]_{tot}) + K_{D,r}([C]_{tot} - [P]_{tot}) + K_{D,r}K_{D,c} \tag{S5}$$

$$c = -K_{D,r}K_{D,c}[P]_{tot} \tag{S6}$$

2. Probe design

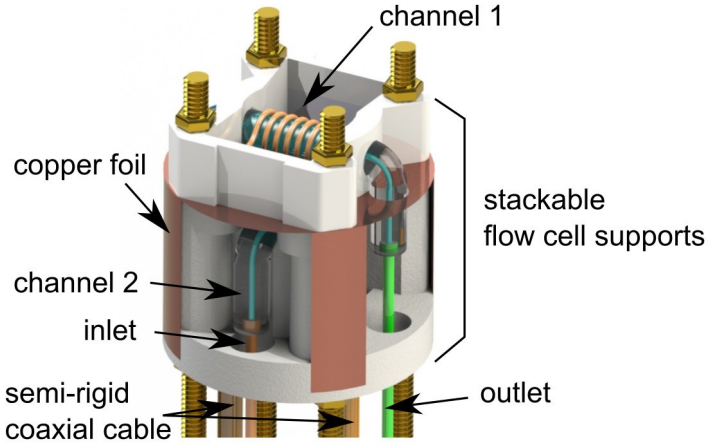

Figure S1. Diagram of the two-channel NMR probe. A 6-turn solenoidal coil is wound around a flow cell, pre-tuned to 376.4 MHz using a fixed capacitor, and connected to a semi-rigid coaxial cable placed next to the coil end. The flow cells are arranged perpendicular to each other, and a copper foil is inserted between the two coils, to minimize a coupling between the coils. The extended legs of this copper foil are in contact with the probe shield to be grounded. Flow cell supports are stackable, enabling to adjust the location of the coils and to add additional cells.

3. Data processing of spin-echo FID

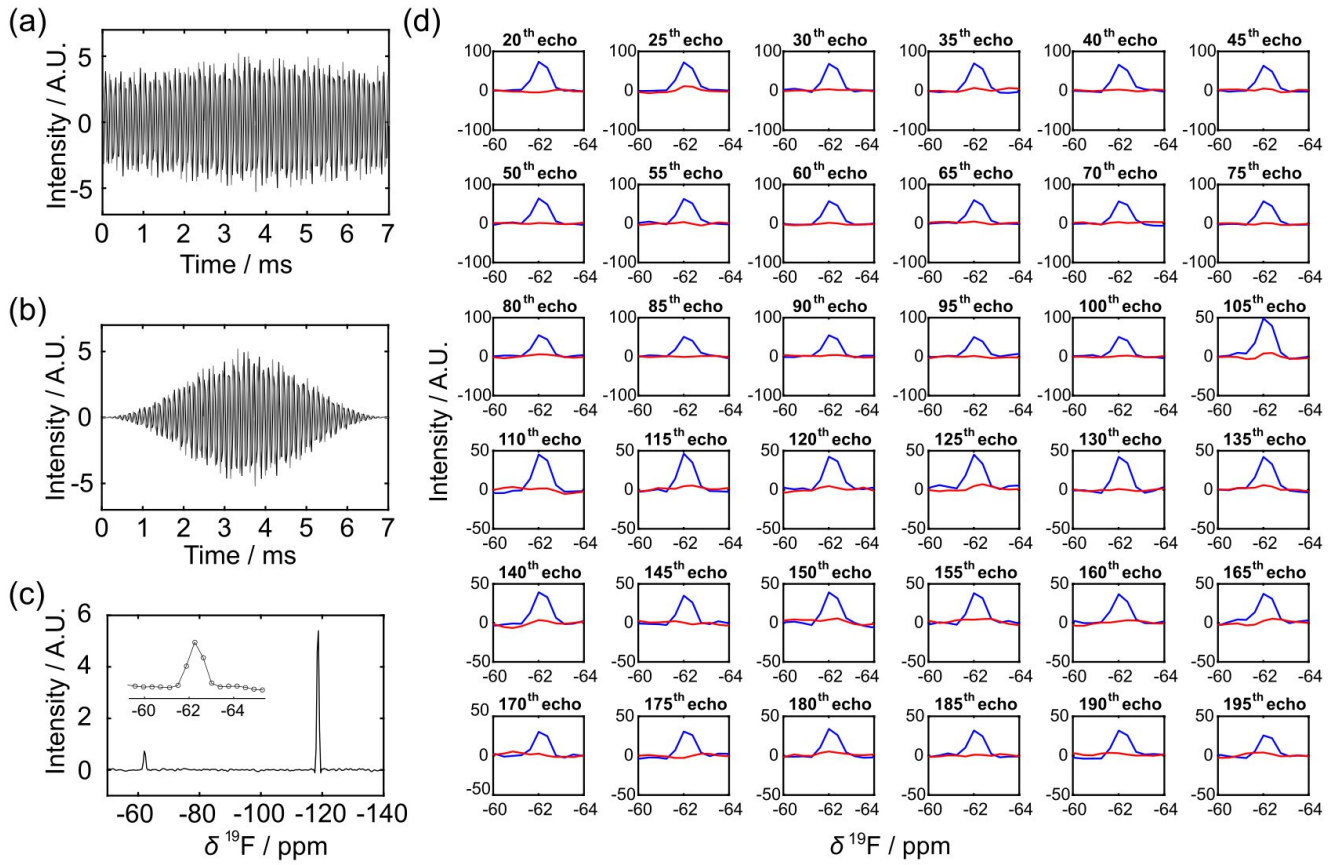

Figure S2. Data processing of the spin-echo FID. (a) Real part of spin-echo from the CPMG experiment of hyperpolarized TFBC and KF. (b) Spin echo apodized with sine-squared window function. (c) Resulting frequency-domain spectrum after Fourier transformation (The inset shows the digital resolution of 0.38 ppm/point). (d) The spectra of successive spin-echoes were properly phased to maximize the real and minimize the imaginary components, shown in blue and red, respectively. The same phase parameters were applied to all spectra.

4. ^{19}F spectra of reference compounds without DNP hyperpolarization

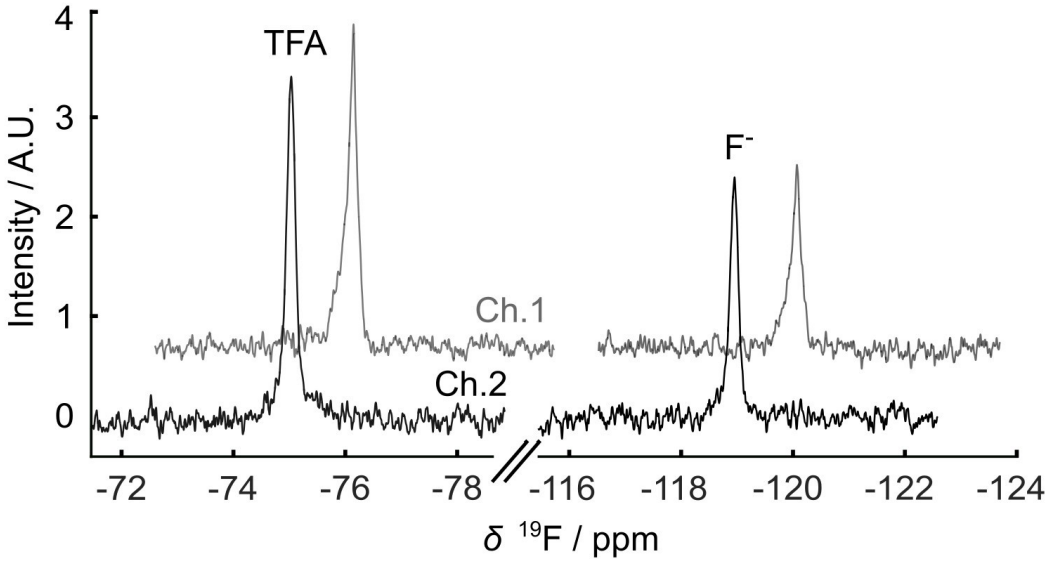

Figure S3. Examples of ^{19}F NMR spectrum acquired under thermal condition after CPMG experiments. Each spectrum is an average of 36 scans. The signals of reference compounds, TFA (δ = –75.0 ppm) and F^- (δ= –118.7 ppm) were used to quantify the final concentrations of hyperpolarized and non-polarized samples in the flow cells. The top and bottom spectra were obtained from Channel 1 and 2, respectively.

5. R_2 relaxation decays of hyperpolarized TFBC from competitive binding experiments

(1) Benzamidine

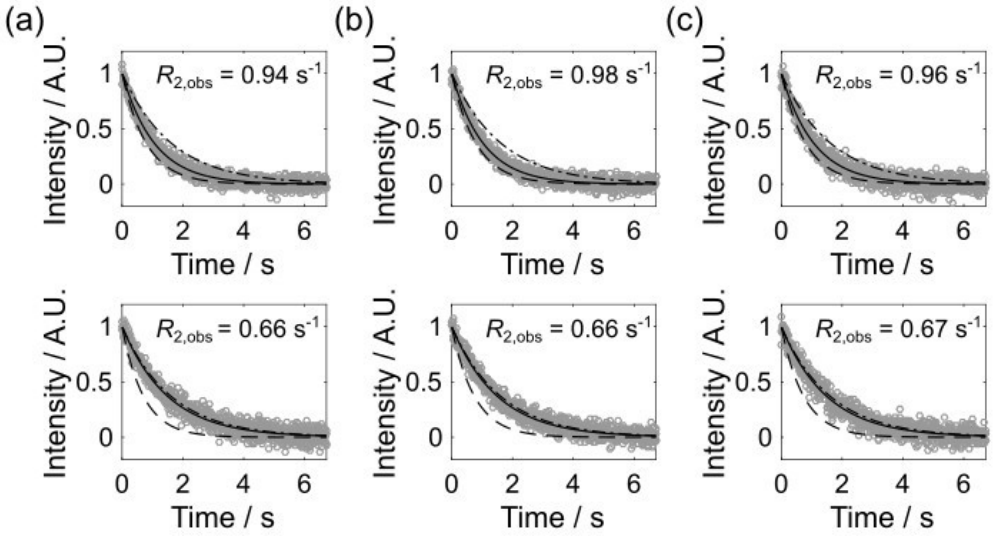

Figure S4. R_2 relaxation decays of hyperpolarized TFBC competing with benzamidine obtained from three CPMG experiments. Each column (a, b and c) represents the same experiment and each row represents the data sets acquired from Channel 1 and 2 at top and bottom, respectively. The TFBC signals from 840 successive spin-echoes are shown using gray circles. The fitted curves are indicated by solid lines and the values of $R_{2,obs}$ are shown in each graph. Limiting curves for free TFBC ($R_{2,f}$ = 0.62 s^{-1}) (– - –) and maximally bound TFBC, calculated from $R_{2,b}^{*}$, (– –) are shown. Data sets in Figure 3a and 3b correspond to those in column (a). The final sample concentrations are summarized in Table S1.

Table S1. Final protein and ligand concentrations

Entry	Channel 1	Channel 2
(a)	[TFBC] = 17.1 μM, [trypsin] = 0.26 μM, [benzamidine] = 13.1 μM	[TFBC] = 17.7 μM, [trypsin] = 0.27 μM, [benzamidine] = 272 μM
(b)	[TFBC] = 17.9 μM, [trypsin] = 0.26 μM, [benzamidine] = 13.1 μM	[TFBC] = 17.5 μM, [trypsin] = 0.24 μM, [benzamidine] = 245 μM
(c)	[TFBC] = 17.4 μM, [trypsin] = 0.26 μM, [benzamidine] = 12.9 μM	[TFBC] = 13.9 μM, [trypsin] = 0.25 μM, [benzamidine] = 246 μM

The entry letters correspond to Figure S4.

(2) Benzylamine

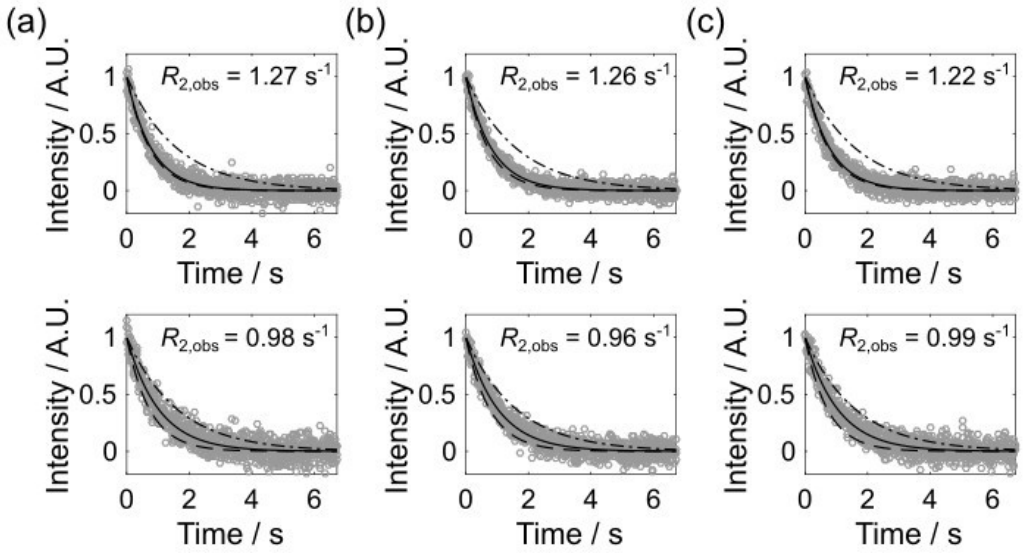

Figure S5. R_2 relaxation decays of hyperpolarized TFBC competing with benzylamine obtained from three CPMG experiments. Each column (a, b and c) represents the same experiment and each row represents the data sets acquired from Channel 1 and 2 at top and bottom, respectively. The TFBC signals from 840 successive spin-echoes are shown using gray circles. The fitted curves are indicated by solid lines and the values of $R_{2,obs}$ are shown in each graph. Limiting curves for free TFBC ($R_{2,f}$ = 0.62 s^{-1}) (– - –) and maximally bound TFBC, calculated from $R_{2,b}^{*}$, (– –) are shown. Data sets in Figure 3c and 3d correspond to those in column (a). The final sample concentrations are summarized in Table S2.

Table S2. Final protein and ligand concentrations

Entry	Channel 1	Channel 2
(a)	[TFBC] = 23.1 μM, [trypsin] = 0.31 μM, [benzylamine] = 15.6 μM	[TFBC] = 18.3 μM, [trypsin] = 0.26 μM, [benzylamine] = 258 μM
(b)	[TFBC] = 23.1 μM, [trypsin] = 0.31 μM, [benzylamine] = 15.3 μM	[TFBC] = 19.1 μM, [trypsin] = 0.27 μM, [benzylamine] = 269 μM
(c)	[TFBC] = 19.8 μM, [trypsin] = 0.32 μM, [benzylamine] = 16.2 μM	[TFBC] = 15.1 μM, [trypsin] = 0.23 μM, [benzylamine] = 233 μM

The entry letters corresponds to Figure S5.

6. R_2 relaxation decays of hyperpolarized TFBC without protein

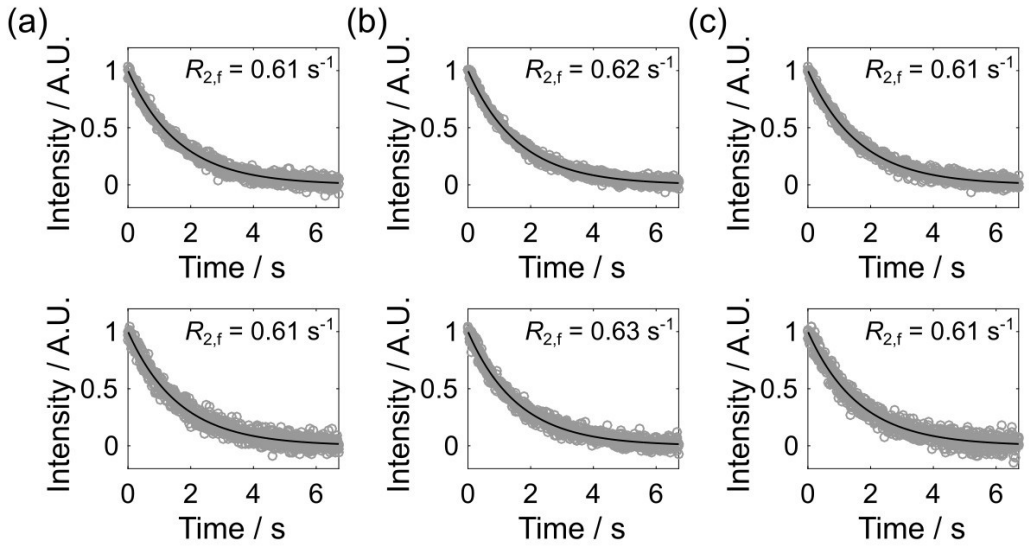

Figure S6. R_2 relaxation decays of hyperpolarized TFBC obtained from three CPMG experiments without admixing any protein. Each column (a, b and c) represents the same experiment and each row represents the data acquired from Channel 1 and 2 in top and bottom panels, respectively. The TFBC signals from 840 successive spin-echoes are shown using gray circles. The fitted curves are indicated by solid lines and the values of $R_{2,f}$ are shown in each graph. The average TFBC concentration was 19.9±2.3 μM.

7. R_2 relaxation decays of hyperpolarized TFBC for $R_{2,b}^*$ measurements

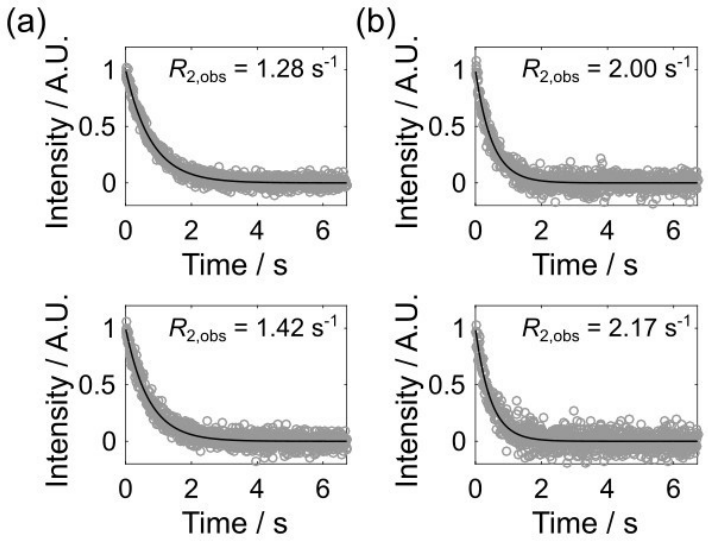

Figure S7. Example data of R_2 relaxation decays of hyperpolarized TFBC obtained from two CPMG experiments admixing 2 μM (a) and 4 μM (b) trypsin solutions. The TFBC signals from 840 successive spin-echoes are shown using gray circles. The data acquired from Channel 1 and 2 are shown in the top and bottom panels, respectively. The fitted curves are indicated by solid lines and the values of $R_{2,obs}$ are shown in each graph. The final sample concentrations are summarized in Table S3.

Table S3. Final protein and ligand concentrations and $R_{2,obs}$

Entry	Channel 1	Channel 2
(a)	[TFBC] = 16.7 μM, [trypsin] = 0.25 μM R_2 = 1.28 s^{-1}	[TFBC] = 18.9 μM, [trypsin] = 0.27 μM R_2 = 1.42 s^{-1}
(b)	[TFBC] = 16.2 μM, [trypsin] =0.52 μM R_2 = 2.00 s^{-1}	[TFBC] = 17.2 μM, [trypsin] = 0.51 μM R_2 = 2.17 s^{-1}
(c)	[TFBC] = 22.9 μM, [trypsin] =0.33 μM R_2 = 1.29 s^{-1}	[TFBC] = 18.3 μM, [trypsin] = 0.25 μM R_2 = 1.32 s^{-1}
(d)	[TFBC] = 19.6 μM, [trypsin] =0.57 μM R_2 = 1.95 s^{-1}	[TFBC] = 17.7 μM, [trypsin] = 0.51 μM R_2 = 2.18 s^{-1}
(e)	[TFBC] = 17.4 μM, [trypsin] =0.51 μM R_2 = 1.87 s^{-1}	[TFBC] = 19.1 μM, [trypsin] = 0.27 μM R_2 = 1.41 s^{-1}
(f)	[TFBC] = 20.5 μM, [trypsin] =0.30 μM R_2 = 1.31 s^{-1}	[TFBC] = 19.5 μM, [trypsin] = 0.59 μM R_2 = 2.07 s^{-1}

A total of 6 CPMG experiments were performed admixing the hyperpolarized TFBC to 2 μM and 4 μM trypsin solutions. The first four entries summarize the results obtained when the same solutions were injected into both channels (a and c: 2 μM trypsin; b and d: 4 μM trypsin), while the last two entries summarize the results obtained when different solutions were used. (e: 4 μM trypsin in Channel 1, and 2 μM trypsin in Channel 2; f: the opposite order of (e)). The entries (a) and (b) correspond to Figure S7.

8. The $K_{D,c}$ values of benzamidine and benzylamine, and the errors assessed using Monte Carlo method

Table S4 –S5. Numerical values for $K_{D,c}$ of benzamidine (1) and benzylamine (2) determined by individual and group fitting methods. The results from the error analysis using the Monte Carlo method are summarized. The entry letters correspond to Figure S4 and Table S1 for benzamidine, and Figure S5 and Table S2 for benzylamine.

(1) Benzamidine

Table S4. Numerical values of $K_{D,c}$ of benzamidine obtained from the original data and error analysis.

Benzamidine		$K_{D,c}$ (μM) ─ Individual fitting				$K_{D,c}$ (μM) ─ Group fitting
		Channel 1		Channel 2		
Entry	Symbol	Data	Simulation (mean $K_{D,c}$, 95% interval)	Data	Simulation (mean $K_{D,c}$, 95% interval)	Data
(a)	◊	11.9	12.1, (8.3, 19.6)	14.2	14.0, (8.5, 21.2)	12.1
(b)	□	14.2	14.6, (9.6, 25.0)	13.6	13.4, (8.2, 20.4)	13.8
(c)	○	11.7	11.9, (8.1, 19.4)	15.1	14.9, (9.2, 22.5)	12.1

(2) Benzylamine

Table S5. Numerical values of $K_{D,c}$ of benzylamine obtained from the original data and error analysis.

Benzamidine		$K_{D,c}$ (μM) ─ Individual fitting				$K_{D,c}$ (μM) ─ Group fitting
		Channel 1		Channel 2		
Entry	Symbol	Data	Simulation (mean $K_{D,c}$, 95% interval)	Data	Simulation (mean $K_{D,c}$, 95% interval)	Data
(a)	◊	107	103, (36.7, 554)	212	215, (151, 328)	204
(b)	□	104	102, (35.8, 580)	182	184, (133, 269)	176
(c)	○	51.1	56.6, (26.0, 235)	226	230, (159, 360)	196

References

(1) Wang, Z.-X. *FEBS Lett.* **1995**, *360* (2), 111–114.